

The Absence of Cold Dust and the Mineralogy and Origin of the Warm Dust Encircling BD +20 307

A. J. Weinberger

Department of Terrestrial Magnetism, Carnegie Institution of Washington

5241 Broad Branch Road NW, Washington, DC 20015

weinberger@dtm.ciw.edu

E. E. Becklin

Department of Physics and Astronomy, University of California Los Angeles

Box 951547, Los Angeles, CA 90095-1562

becklin@astro.ucla.edu

I. Song

Department of Physics and Astronomy, The University of Georgia

Athens, GA 30602-2451

song@uga.edu

B. Zuckerman

Department of Physics and Astronomy, University of California Los Angeles

Box 951547, Los Angeles, CA 90095-1562

ben@astro.ucla.edu

ABSTRACT

Spitzer Space Telescope photometry and spectroscopy of BD +20 307 show that all of the dust around this remarkable Gyr-old spectroscopic binary arises within 1 AU. No additional cold dust is needed to fit the infrared excess. Peaks in the 10 and 20 μm spectrum are well fit with small silicates that should be removed on a timescale of years from the system. This is the dustiest star known for its age, which is $\gtrsim 1$ Gyr. The dust cannot arise from a steady-state collisional cascade. A catastrophic collision of two rocky, planetary-scale bodies in the terrestrial zone is the most likely source for this warm dust because it does not require a reservoir of planetesimals in the outer system.

1. Introduction

A number of extreme collisions may have shaped the final states of the terrestrial planets. Impact by a Mars-sized progenitor on the early Earth, perhaps 30 Myr after the Solar System

formed, could have created the Moon (e.g. Canup 2004). Other collisions may have stripped Mercury’s mantle (Benz et al. 1988) or caused the hemispheric crustal thickness asymmetry of Mars (Marinova et al. 2008). Subsequent bombardment of the planets may not have generated planetary scale changes, but the “Late Heavy Bombardment,” an era approximately 600 Myr after Solar System formation, either culminated a long sequence of bombardments or resulted in a burst of impacts on the terrestrial planets (Gomes et al. 2005; Strom et al. 2005).

Evidence of cataclysmic impacts in other planetary systems is rare. Enhanced collisions should result in the production of copious small particles, i.e. dust, which can be observed by their re-radiation of stellar light (Kenyon & Bromley 2004). Stars older than 100 Myr with substantial amounts of warm dust are rare, and at most a few percent of field stars have any detectable warm dust at all (e.g. Meyer et al. 2008; Trilling et al. 2008; Greaves et al. 2009; Koerner et al. 2010). At any given age, stars that are dustier than average could be interpreted as having had a recent, stochastic, event, but many could also be the result of differing initial masses and configurations of planetesimals. Only the extremely dusty disks at any given age must be from giant collisions.

BD+20 307 is a relatively anonymous field star at 96_{-10}^{+13} pc (van Leeuwen 2007) from the Sun. It is actually a tidally locked spectroscopic binary with a period of 3.5 d composed of two nearly identical late F-type stars with a mass ratio of 0.91 (Weinberger 2008). Weinberger (2008) and Zuckerman et al. (2008) investigated the stellar properties, in particular the weak and disparate Lithium abundances in the two stars, and estimated an age $\gtrsim 1$ Gyr. At that age, its dust opacity, estimated by L_{IR}/L_{\star} to be 0.033 (Song et al. 2005), is orders of magnitude larger than every other star of its age. In fact, such dustiness would be extraordinary even for a star 10–100 times younger.

A small class of very (warm) dusty objects now exists in the literature (see summaries in Rhee et al. (2008); Moór et al. (2009)). The extreme examples of these and also some disks with strange infrared spectra such as HD 172555 (Lisse et al. 2009) and 51 Oph; (Ancker et al. 2001), have been attributed to impacts of planet-sized bodies.

Here, we investigate the unusually dusty system around the star BD+20 307 using the Spitzer Space Telescope. These observations constrain the size distribution and location of a very large amount of dust and provide perhaps the best evidence yet for large-scale collisions in another system.

2. Observations and Data Reduction

We observed BD +20 307 with Spitzer with all three instruments – IRAC, MIPS, and IRS. An observing log is given in Table 1.

2.1. IRAC

IRAC data were taken in subarray mode, which yields 64 individual images. The S14 pipeline reduction was used, and the “Basic Calibrated Data” (BCD) images were mosaiced with the Spitzer Science Center’s MOPEX software. There are two photometric corrections to consider. The first is the “Pixel phase dependent photometric correction” that corrects the pixel response function for where the peak response is within a pixel. This correction was applied to channel 1, and amounted

to 1.7%. The second is the array location dependent photometric correction, due to the fact that IRAC is flat-fielded on the Zodiacal spectrum. From the overall shape of the BD +20 307 spectral energy distribution (SED), we know that its spectrum is shallower in slope than Rayleigh-Jeans from 3–7 μm but not as flat as the Zodiacal emission. The correction was applied at Channel 1, and amounted to 0.7%. It was also applied to channels 2 and 3, but made less of an effect, and was not applied for channel 4. Aperture photometry was performed in the radius 2, 3, and 5 pixel radii apertures given in the IRAC handbook, and the standard deviation of these taken as the measurement uncertainty.

Finally, the IRAC data need to be color corrected from the default $\nu F_\nu = \text{constant}$ calibration to the true BD+20 307 spectrum. This effect is small for Bands 1 and 2, where the source spectrum is approximately a 1000 K blackbody, and the correction is 0.7%. For bands 3 and 4, we integrated the observed IRS spectrum over the IRAC filter bandpasses. This yields a correction of 3% at Band 3 and 71% for Band 4. The Band 4 correction is unreasonably large; the difference between the integral under the IRS spectrum and the IRAC Band 4 (un-color corrected) flux density is only 26%. When integrated, the very large spectral slope at 8 μm due to the silicate feature that peaks at $\approx 10 \mu\text{m}$, causes a large change in color correction for any small change in spectral transmission response of the system (telescope + filter, etc.). This transmission does not appear to be well enough known to provide an accurate color correction; therefore, the Band 4 flux was not used for further analysis.

2.2. MIPS

At 24 μm , the pipeline produced post-BCD mosaic was used for aperture photometry using a 6 pixel aperture and corrections given in Su et al. (2006). At 70 μm , MOPEX was used to mosaic the pipeline filtered BCDs. Aperture photometry was performed with the 35" aperture and corrections from Gordon et al. (2007). At 160 μm , the pipeline mosaic was used. Because at this band no

Table 1. Summary of Observations and Photometry

Instrument	Band	Date	Integr. time (s)	Photometry (mJy)
IRAC	1 (3.5 μm)	2005-08-20	0.64	285.0 \pm 7.3
IRAC	2 (4.5 μm)	2005-08-20	0.64	210.4 \pm 4.8
IRAC	3 (5.7 μm)	2005-08-20	0.64	165.3 \pm 12.0
IRAC	4 (7.9 μm)	2005-08-20	0.64	410.2 \pm 22.5 ^a
MIPS	1 (24 μm)	2007-01-21	2.62	441.0 \pm 0.8
MIPS	2 (70 μm)	2007-01-21	167.8	28.6 \pm 1.9
MIPS	3 (160 μm)	2007-01-21	209.8	<22
IRS	0 (5.2–14.5 μm)	2006-01-15	12.6	–
IRS	1 (9.9–19.6 μm)	2006-01-15	188.7	–
IRS	3 (18.7–37.2 μm)	2006-01-15	1219	–

^aNot color corrected

source is seen at the nominal location or elsewhere in the field, an upper limit to the source flux was placed by doing a raster of aperture positions on the image around the nominal location and calculating three times the standard deviation of these.

2.3. IRS

For all channels, the pipeline version 14 data were used. The short-low ($5.2 - 14.5 \mu\text{m}$) BCD data were cleaned with IRS_CLEAN software to remove bad pixels. Each cleaned BCD was sky subtracted with uncertainties propagated in quadrature. The spectra were extracted with the Spitzer Science Center’s SPICE software using the standard extraction parameters.

The short-high ($9.9 - 19.6 \mu\text{m}$) BCD data were cleaned with IRS_CLEAN and the unaltered campaign pixel mask. The resulting cleaned BCDs were medianed to make a final spectrum that was extracted with SPICE and the standard extraction parameters. The two nods were averaged together. Orders were trimmed to eliminate as many points with undefined uncertainties as possible.

For the long-high ($18.7 - 37.2 \mu\text{m}$) data, separate observations on nearby sky were taken to help in elimination of rogue pixels. A median sky frame was created with the standard deviation of the 20 sky files as its uncertainty. This frame was then subtracted from each of the object spectra, with uncertainties propagated.

The campaign rogue mask was augmented by any pixels that were flagged in 15/20 of the individual spectra. The combined mask was then used to clean the sky subtracted object spectra. The final cleaned BCDs for each nod were median combined and then extracted with SPICE. The spectra from the two nods, which agree to within their statistical uncertainties, were averaged.

The spectra from all channels were combined by using their overlap regions – short-high to short-low spectrum in the region $11.5-14 \mu\text{m}$ and long-high to short-high at $19.02-19.47 \mu\text{m}$. The complete spectrum was then normalized to the MIPS channel 1 photometry by integrating the spectrum under its transmission curve. A check that this process works well is that integrating the final normalized spectrum under the IRAC channel 3 filter yields 155 mJy compared with the measured $165 \pm 12 \text{ mJy}$ from the photometry reported in Table 1.

3. Results

Results of the new Spitzer photometry are given in Table 1. As first reported in Song et al. (2005), the spectral energy distribution of BD+20 307 at wavelengths longer than $5 \mu\text{m}$ is dominated by emission by small silicate particles. We show the overall SED including the new Spitzer spectrum and photometry along with previous ground-based photometry in Figure 1.

3.1. Photosphere Modeling

We model the combined flux density of the nearly identical central stars with a single Kurucz model atmosphere fit to the Tycho-2 and 2MASS photometry at $0.4 - 2.2 \mu\text{m}$. The best fit model has a gravity of $\log(g)=4.5$, $T_{\text{eff}}=6000$, and, at the parallactic distance of 96 pc , a luminosity of

1.94 L_{\odot} . Zuckerman et al. (2008) finds the luminosity ratio of the two stars as 0.78, which would imply individual luminosities of 1.10 and 0.84 L_{\odot} . Table 2 gives the amount of photosphere in each Spitzer band and the remaining disk flux. The model photosphere was also subtracted from the IRS spectrum.

3.2. Spectral Fitting

We proceed by assuming a simple model for the composition and location of the circumstellar dust and asking whether it is a plausible match to the data. The presence of both broad and sharp spectral features indicates emission by both amorphous and crystalline materials (e.g. Campins & Ryan 1989).

The shortest observed peak, at 9.7 μm , is matched well by the wavelength of the peaks in measurements of glassy silicates, although its width is narrower than that produced by even very small ($\lesssim 0.1 \mu\text{m}$) grains. The breadth of the 16-20 μm peak is better fit by larger, 1 μm grains. We chose to set the minimum grain size to 0.5 μm , which is approximately the blow-out size for radiation pressure from the stars. We then use a power law distribution of sizes rising from 0.5 μm with slope -3.5, but the fit does not materially change whether the power law distribution or just the minimum-sized grains are used. Smaller grains result in narrower peaks that improve the fit at 10 μm but make it worse at 20 μm .

We take the simple model to be dust at a single distance from the star and composed of four types of particulates: small amorphous dust of olivine composition (MgFeSiO_4 ; hereafter called amorphous olivine), small crystalline olivine (forsterite; Mg_2SiO_4), small amorphous pyroxenes ($\text{Mg}_{0.5}\text{Fe}_{0.5}\text{SiO}_3$), and large grains (i.e. those that behave as blackbodies). These are common constituents used to model solar system comets and circumstellar disks (e.g Li et al. 2004).

All small particles (size \ll wavelength of observation) have absorption efficiencies that fall faster than Rayleigh-Jeans (i.e. $\propto \lambda^{-2}$) at wavelengths much larger than the particle size. Therefore, some bigger grains are necessary to match the measured flux densities at 20–70 μm . Again, as a matter of taste, we have chosen to keep the grain size distributions for the olivines and pyroxenes the same, as that seems the most likely physical outcome of a collisional cascade, and introduce a blackbody component to the fit. The minimum size of the pyroxenes is not well-constrained by the

Table 2. Photosphere subtracted flux densities and model fits in mJy

Band	Photosphere	Disk flux	Model (mJy)
IRAC1	261.0	24.0	9.3
IRAC2	167.0	43.4	28.8
IRAC3	107.1	58.2	70.8
IRAC4	60.7	349.5	293.2
MIPS1	6.8	434.2	424.4
MIPS2	0.8	27.8	40.2
MIPS3	0.3	<22	8.7

shape of the spectrum, because pyroxenes have relatively broad features. A larger minimum size for the amorphous pyroxenes could be traded off against the blackbody grain component.

We assume that the disk dust is optically thin, so that each dust grain is in thermal equilibrium based on its own absorption efficiency and that the various emission components simply add. The Spitzer 3.5, 4.5, 5.7, and 70 μm photometry and the combined 5.6 – 25 μm spectrum are fit simultaneously.

We write the emission due to the disk dust in the optically thin case as:

$$F_\nu = \Sigma A_i \kappa_i B_{\nu,i}(d) \quad (1)$$

where the sum is over i independent dust species each with their own mass absorption coefficients, $\kappa_i = 3Q_{abs}/4a\rho$ where Q_{abs} is the absorption efficiency, a is the grain radius, and ρ is the grain density. The dust grains are not assumed to be in thermal contact; thus each species has its own temperature determined by its Q_{abs} , distance from the star, and the luminosity of the star by assuming it is in thermal equilibrium. These temperatures are calculated self-consistently by making distance from the star the free parameter. The other free parameters are the number or surface density of dust grains of each type, i.e. the A_i .

A major choice is what absorption efficiencies to use. Various authors have taken different approaches to this problem. Because we do not leave temperature as the free parameter, we need genuine ultraviolet and visible absorption efficiencies, as this is where the star emits and the grains absorb most efficiently, in order to calculate temperatures. For this reason, we opt for Mie calculations.

Mass absorption efficiencies from the group at Kyoto Pharmaceutical University (Koike et al. 2000; Sogawa et al. 2006, e.g.) are available only in the infrared. Optical constants from the Jena group are provided into the UV-visible, but are only accurate in the near-infrared and longer (Dorschner et al. 1995, e.g.). For the amorphous olivine, we adopted the optical constants of Li et al. (2004) which combine the Jena measurements with ultraviolet data. We then used a Mie code¹ to calculate the mass absorption opacities.

For crystalline olivine, shape is a major determinant of spectrum. The Jena group has measured the triaxial indices of refraction, but how one uses these to calculate the absorption is a matter of taste. Assumption of spherical particles results in sharp peaks that are not observed (Fabian et al. 2001). The Jena group provides two computations of continuous distributions of ellipsoids (CDE) in the Rayleigh limit. We combined these with the ultraviolet efficiencies calculated in the Mie limit from the constants of Li et al. (2004). We tested both the CDE1 (weighted toward spherical grains) and CDE2 (all shapes weighted equally) calculations against our spectra and found that CDE1 was a better match. It is also CDE1 that fairly closely matches a real grain measured in the Jena laboratory (Fabian et al. 2001).

It is because of the flexibility in spectral shape granted by choosing the exact distribution of grain shapes, that we have not attempted a multi-component fit that would reduce our chi-square to a level approximately equal to one. We believe that the large number of free parameters to

¹<http://www-atm.physics.ox.ac.uk/code/mie/index.html>

choose from makes this exercise of limited value.

To find the best fit, we compare the model excess as described above to the photometric (2.16 – 70 μm) points and IRS spectrum in the classic χ^2 formalism. We first perform a search over a large range of parameter space for the free parameters using the Amoeba routine from Numerical Recipes (Press et al. 1992) as implemented in IDL. Once the best fit has been found, we then loop over a small range of values for the free parameters to determine the shape of the χ^2 and determine a better minimum.

The best fit is shown in Figure 2. The best distance to the dust is 0.85 AU from the star. The calculated temperatures of the grains are 461 K for the pyroxene, and 460 and 507 K for the amorphous and crystalline olivine silicates, respectively. The blackbody temperature is 358 K. The reduced chi-square value of this fit is 19.7. Obviously, the reduced chi-square is not near one, but nonetheless, the fit is capable of explaining all of the main features of the spectrum including the excess emission at 3–5 μm the whole of the 70 μm emission, and the locations of peaks ((10, 12, 17, 19, and 24 μm) in the 7–35 μm spectrum. The overall match between spectrum and the model is good except in the heights of the peaks at 10 and 17 μm and the continuum at 25–30 μm . For the issues of most relevance, namely the temperature of the dust, the presence of small grains, and the crystallinity fraction, this model adequately represents the spectrum. Its predictions in the various filters are given in Table 2. The best fit parameters are given in Table 3.

The contributions by mass are 50% amorphous olivines, 30% amorphous pyroxenes, and 20% crystalline olivines. The actual masses in these small grains range from 0.7 to 1.7×10^{22} g. Obviously, most of the mass would be in the blackbody grains. A minimum mass for these can be set by setting the minimum grain radius for one of the above grains to look like a blackbody, or ~ 30 μm . Then, the minimum mass is 6×10^{23} g.

4. Discussion

The remarkable results of the Spitzer data are the lack of cold dust – all of the 70 μm emission arises from the same close-in population of dust producing the bright 8 – 30 μm silicate features, and that the dust that does orbit the star is extremely close-in – within 1 AU. It is the most dusty

Table 3. Best Fit Model

colheadComponent	A_i	T (K)	L_{IR}/L_*
Amor. Olivine	1.0 ^a	460	0.010
Amor. Pyroxene	0.653 ^a	462	0.006
Crys. Olivine	0.821 ^a	508	0.004
Blackbody	1.64e-4	358	0.011
distance	0.85 AU	–	–

^aThese coefficients, defined in Section 3.2, are normalized such that Amor. olivine is 1.0.

star for its age known and the one with the warmest dust.

There are now about ten known “warm” debris disks around FGK stars (Rhee et al. 2008; Moór et al. 2009; Fujiwara et al. 2010; Melis et al. 2010). Most of these have dust temperatures of $\sim 150\text{--}200$ K and $L_{IR}/L_* < 5 \times 10^{-4}$. For stars older than 1 Gyr, BD +20 307 has more than two orders of magnitude more dust opacity than the others. The closest star in terms of dustiness is the much younger Pleiades member HD 23514.

The timescale over which the BD+20 307 disk should evolve are short. The treatment of radiation pressure on small silicates in Burns et al. (1979) and scaled to the slightly larger mass and luminosity of BD+20 307 suggests that all grains smaller than $0.5 \mu\text{m}$ will be blown away on an orbital timescale, which at 0.85 AU, assuming a central mass of $2.2 M_\odot$, is 0.5 yr.

Taking the model fit $L_{IR}/L_* = 0.032$ as the surface density of the grains yields a collision time of 2.4 yr. This is only a few times longer than the orbital time, so the small grains observed in the spectrum will be created and then lost nearly immediately. Wyatt et al. (2007) argue that massive planetesimal belts grind themselves down by collisions quickly, so it is not possible to maintain very large amounts of dust in the terrestrial planet region of old stars. They included BD+20 307 in the list of stars for which it was impossible to generate the present dust through collisional grinding, even using the IRAS 60 μm upper limit to constrain the cold planetesimal population and for an age of 300 Myr. At the current best estimate of its age of at least 1000 Myr, its maximum L_{IR}/L_* in steady state (see their Eq. 20) is 7.4×10^{-8} . Recently, Heng & Tremaine (2010) confirm the Wyatt et al. (2007) result that BD +20 307 cannot be from a steady-state collisional cascade, although their models allow most of the other warm disk sources to come from a warm planetesimal cascade.

We do not detect any cold dust; our best-fit model for the hot dust actually overpredicts the measured 70 μm flux density and is slightly higher than the 1σ upper limit at 160 μm (Figure 3). A check on the reasonableness of the lack of cold dust, is that if we take the average flux density in the IRS spectrum of 0.4 Jy and extrapolate this as a Rayleigh-Jeans fall-off from the mean wavelength of the IRS spectrum, 20 μm , we would predict a 70 μm flux density of 0.032 Jy, which is again higher than measured.

We can place a conservative upper limit on the amount of cold dust by finding the luminosity of a dust ring whose spectrum peaks at 160 μm (i.e. temperature of 33 K) and produces no more than a 10% increase in the flux density at 70 μm – such a cold disk would produce an additional 6 mJy at 160 μm , which would still fall under the measured 3σ upper limit and would have a $L_{IR}/L_* = 3 \times 10^{-5}$. Therefore, in the context of the Wyatt et al. model for planetesimal belt self-grinding, the lack of detectable cold dust rules out any belt within 200 AU that is losing mass at a rate sufficient to account for the hot dust.

Late heavy bombardment models per se are not attractive analogies for BD+20 307. In the (Gomes et al. 2005) scenario, a late crossing of the 2:1 resonance between Jupiter and Saturn swept resonances across the asteroid and Kuiper belts and dislodged many small bodies that then impacted the terrestrial planets. For a similar scenario to work for BD+20 307, the resonance crossing must be delayed even longer, until 1 Gyr, but that is likely achievable by tuning the initial configuration of planets. More problematic is that the Kuiper Belt prior to the late heavy bombardment, which was massive enough to generate giant planet migration, would itself produce significant cold dust (Meyer et al. 2007).

The remaining hypothesis for the source of the hot dust around BD+20 307 is a giant impact. Detailed models exist of one such impact – the Moon-forming event. About a quarter of the material that forms the circum-terrestrial disk out of which the Moon formed starts very hot, at temperatures >1000 K, or high enough to vaporize silicates and metals (Canup 2004). Furthermore, a few percent or more of a Lunar mass can escape the Earth-Moon system. The small particles around BD+20 307 are $\sim 20\%$ crystalline. This level of crystallinity is well within range of T Tauri star dust; in contrast, differentiated bodies such as large asteroids or planets should be nearly 100% crystalline. That the observed dust is largely amorphous suggests that the impact heated the bulk of the material to temperatures ~ 1000 K and that any recondensation took place under low vapor pressure conditions where the molten silicate cooled quickly and therefore did not re-anneal into crystalline form.

A terrestrial planet system may be stable over a Gyr but not permanent. The Planet V models of Chambers (2007) show that in a configuration such as the Solar System’s, a fifth planet can survive in the inner Solar System for a Gyr and create collisions of terrestrial planets at many hundreds of millions of years after the system formed. The configuration of the exoplanet system will determine how long it lasts; small planets further from the star take longer to go unstable (Chambers, personal communication). In the case where a tenuous asteroid belt still remains in a planetary system, the trajectory of a rogue planet can destabilize the belt and produce collisions between planetesimals or bombardment of the planets. Over several Gyr, our current terrestrial planet system may be unstable and result in collisions between the planets (Laskar & Gastineau 2009).

Recently, Matranga et al. (2010) suggested that the changing separation of close binaries due to angular momentum loss could sweep resonances across planetary systems and destabilize their planetesimal belts. The stars in BD+20 307 are separated by 0.06 AU at present Weinberger (2008), and thus the disk radius is $14\times$ the binary separation. They have likely been in a tight circular orbit for billions of years Weinberger (2008) and their relatively low X-ray activity likely makes their angular momentum loss relatively slow.

How common are giant collisions amongst sun-like stars? We can estimate the number of giant impacts per star $N_g = f_*AL^{-1}$ where f_* is the fraction of stars observed to have hot dust, L is the lifetime of the collision products, and A is the age of the stars surveyed.

To estimate the lifetime of the dust, we invert the (Wyatt et al. 2007) expression for the amount of dust that can be produced by a collisional cascade over time (their equation 20) to solve for the lifetime of a collision that starts in a giant impact. The most significant unknown is the internal strength of the large planetesimal(s) involved, but the binding energy is likely closer to that of a differentiated planet than a pure rubble pile, i.e. more like 2×10^5 than 200 J kg $^{-1}$. Therefore, a planet-sized impact could generate a cascade that lasts up to 80,000 yr. This result is similar to the 100,000 yr lifetime for a collisional cascade started by planetary embryos as calculated by (Melis et al. 2010).

Surveys with Spitzer have looked at all Sun-like stars within 25 pc Koerner et al. (2010), for a sample of about 800. The average age of this population is $\gtrsim 3$ Gyr but it includes a small fraction of much younger stars (Wright et al. 2004). While there are five stars with warm dust in this sample, we note that these have $24 \mu\text{m}$ flux densities $\lesssim 10$ times their photospheres and $L_{\text{IR}}/L_\star \lesssim 10^{-3}$, and so are not nearly as extreme as BD+20 307. Moreover, their average age is < 1 Gyr.

Their warm dust may either be from young planetesimal belts (e.g. β Pic, which is in this group) or from collisions fed by outer belts and constrained by planets (e.g. η Corvi; Wyatt et al. 2007).

IRAS was capable of detecting every A–G star with as much hot dust as BD+20 307 out to ~ 280 pc, although it is possible some of these would not have been noticed. There are $\sim 600,000$ stars of earlier spectral type than K0 in that volume. Four stars (including BD +20 307) have $F_{24}/F_* > 10$. This fraction of host dust stars implies a giant impact rate greater than 0.2 impacts/star during its main sequence lifetime, i.e. implies that such impacts are common. Obviously, these are small number statistics. The WISE mission currently surveying the sky at mid-infrared wavelengths will greatly improve the statistics. Its sensitivity is 500 times better than IRAS at $\sim 24 \mu\text{m}$ (Liu et al. 2008), and so it should provide a truly complete census of isolated hot dust sources out to a few kpc.

It is difficult to search for planets around BD+20 307 with the radial velocity technique because of the spectroscopic binary. However, if planets do encircle this star, they may trap small bodies in resonance. An enhancement in the planetesimal density might increase the likelihood of a destructive collision such as the one observed. The star HD 69830, also an IRAS source, and > 1 Gyr old, was shown with Spitzer to harbor a ring very similar in size and temperature to that around BD+20 307, but containing 150 times less dust (Beichman et al. 2005). A system of three Neptune mass planets was then found to encircle HD 69830, with the dust either residing between the 2nd and 3rd planets from the star or exterior to all three (Lovis et al. 2006).

Whatever the scenario that originated the collision in the BD+20 307 system and others, it is interesting to note that the spectra of other warm dust systems are not identical. HD 69830, for example, has much more prominent $20 \mu\text{m}$ crystalline silicate peaks (Beichman et al. 2005) and HD 23514 has an unusual broad spectral feature at $9 \mu\text{m}$ rather than $10 \mu\text{m}$ (Rhee et al. 2008). HD 172555’s narrow $8 \mu\text{m}$ peak and featureless $20 \mu\text{m}$ regions have been attributed to SiO. These various compositions may result from a combination of progenitor composition, which would affect the primordial abundances of different types of silicates, and geometry of the impact, which can change the melt fraction and condensation properties of its debris.

5. Conclusions

We have detected a large amount of small silicate dust at 0.85 AU from the $>$ Gyr old star BD+20 307 but no cold dust that could be generated tens or hundreds of AU from the star. A catastrophic collision of two rocky, planetary-scale bodies in the terrestrial zone is the most likely source for this warm dust because it does not require a reservoir of planetesimals in the outer system. Furthermore, the high amorphous silicate content of the dust suggests that the impact must have caused a high melt fraction and amorphization of what was likely a largely crystalline parent body.

This work is based on observations made with the Spitzer Space Telescope, which is operated by the Jet Propulsion Laboratory, California Institute of Technology under a contract with NASA. Support for this work was provided by NASA through an award issued by JPL/Caltech and a contract to Ames Research Center for the SOFIA program. We acknowledge support from NASA’s Astrobiology Institute to the UCLA and CIW nodes. John Chambers and Sarah Stewart provided

insightful conversations on the topic of giant impacts.

REFERENCES

- Ancker, M. E. V. D., Meeus, G., Cami, J., Waters, L. B. F. M., & Waelkens, C. 2001, *A&A*, 369, L17
- Beichman, C. A., Bryden, G., Gautier, T. N., Stapelfeldt, K. R., Werner, M. W., Misselt, K., Rieke, G., Stansberry, J., & Trilling, D. 2005, *ApJ*, 626, 1061
- Benz, W., Slattery, W. L., & Cameron, A. G. W. 1988, *Icarus*, 74, 516
- Burns, J. A., Lamy, P. L., & Soter, S. 1979, *Icarus*, 40, 1
- Campins, H., & Ryan, E. V. 1989, *ApJ*, 341, 1059
- Canup, R. M. 2004, *Icarus*, 168, 433

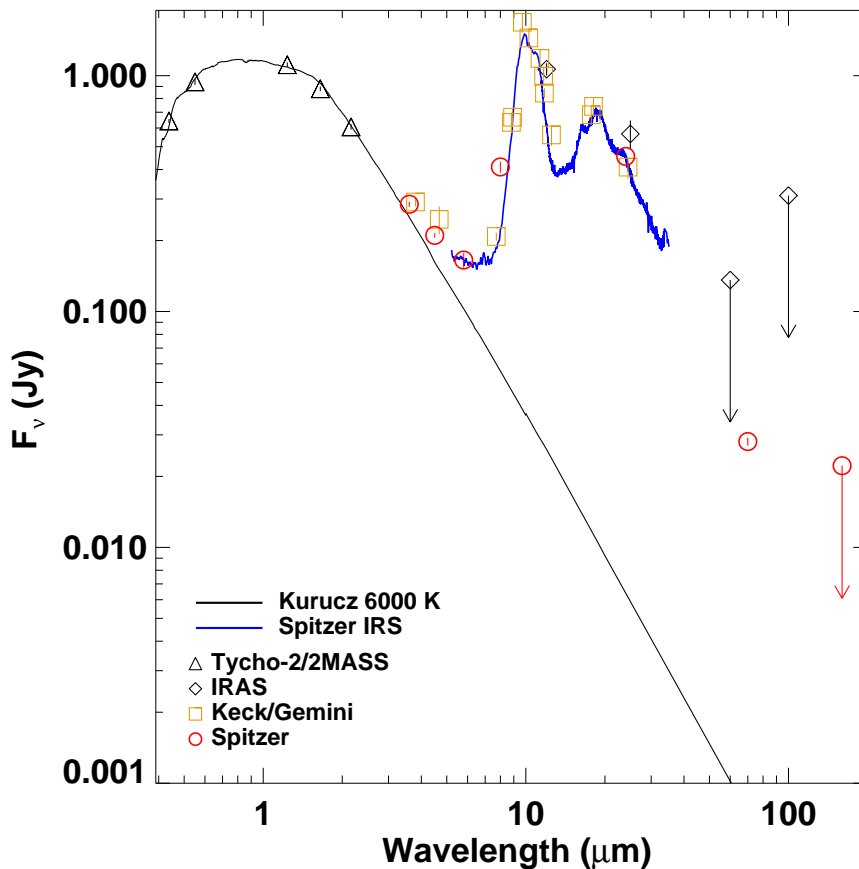


Fig. 1.— Spectral Energy Distribution of BD+20 307. The Tycho-2 and 2MASS points (black triangles) were used to fit the Kurucz photosphere (black line). All long wavelength data are plotted including our Spitzer photometry (red circles) and spectroscopy (blue line) as well as IRAS (black diamonds) and older ground-based data from Song et al. 2005 (gold squares).

Chambers, J. E. 2007, *Icarus*, 189, 386

Dorschner, J., Begemann, B., Henning, T., Jaeger, C., & Mutschke, H. 1995, *A&A*, 300, 503

Fabian, D., Henning, T., JGer, C., Mutschke, H., Dorschner, J., & Wehrhan, O. 2001, *A&A*, 378, 228

Fujiwara, H., Onaka, T., Ishihara, D., Yamashita, T., Fukagawa, M., Nakagawa, T., Kataza, H., Ootsubo, T., & Murakami, H. 2010, *ApJ*, 714, L152

Gomes, R., Levison, H. F., Tsiganis, K., & Morbidelli, A. 2005, *Nature*, 435, 466

Gordon, K. D., Engelbracht, C. W., Fadda, D., Stansberry, J., Wachter, S., Frayer, D. T., Rieke, G., Noriega-Crespo, A., Latter, W. B., Young, E., Neugebauer, G., Balog, Z., Beeman, J. W., Dole, H., Egami, E., Haller, E. E., Hines, D., Kelly, D., Marleau, F., Misselt, K., Morrison, J., Pérez-González, P., Rho, J., & Wheaton, W. A. 2007, *PASP*, 119, 1019

Greaves, J. S., Stauffer, J. R., Cameron, A. C., Meyer, M. R., & Sheehan, C. K. W. 2009, *MNRAS*, 394, L36

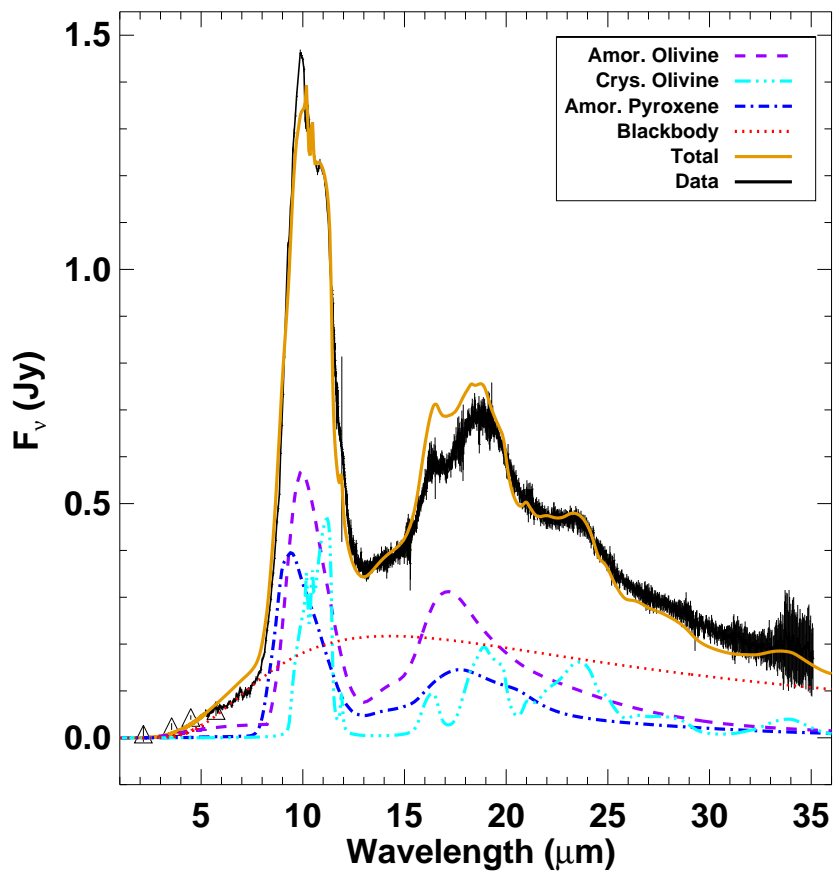


Fig. 2.— Best fit model to the Spitzer spectrum (black line), derived as described in the text. The various dust components (purple: amorphous olivine, cyan: crystalline olivine, dark blue: amorphous pyroxene, and red: blackbody grains) sum to make the total spectrum (gold line). All components are situated at the best fit distance of 0.85 AU.

Heng, K. & Tremaine, S. 2010, MNRAS, 401, 867

Kenyon, S. J. & Bromley, B. C. 2004, ApJ, 602, L133

Koerner, D. W., Kim, S., Trilling, D. E., Larson, H., Cotera, A., Stapelfeldt, K. R., Wahhaj, Z., Fajardo-Acosta, S., Padgett, D., & Backman, D. 2010, ApJ, 710, L26

Koike, C., Tsuchiyama, A., Shibai, H., Suto, H., Tanabé, T., Chihara, H., Sogawa, H., Mouri, H., & Okada, K. 2000, A&A, 363, 1115

Laskar, J. & Gastineau, M. 2009, Nature, 459, 817

Li, M., Zhao, G., & Li, A. 2004, ApJ, 613, L145

Lisse, C. M., Chen, C. H., Wyatt, M. C., Morlok, A., Song, I., Bryden, G., & Sheehan, P. 2009, ApJ, 701, 2019

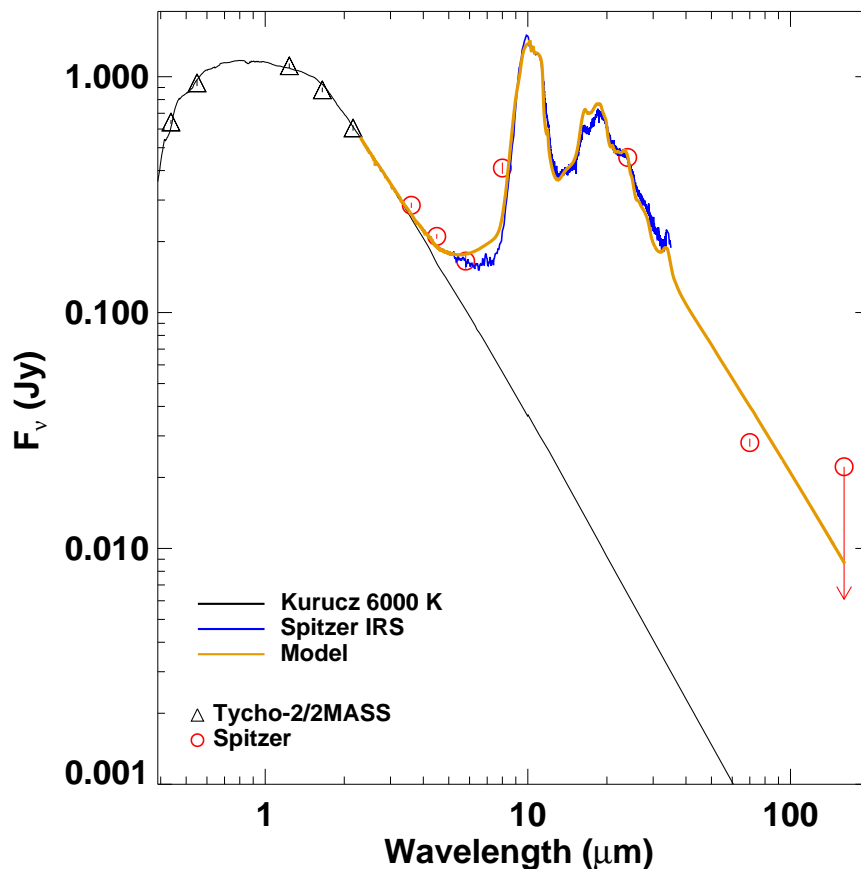


Fig. 3.— Spectral energy distribution of BD+20 307 showing the visual and near-infrared photometry from the Tycho-2 and 2MASS catalogs along with the Spitzer photometry and spectroscopy from Figure 1 and our best-fit model from Figure 2. We do not detect any cold dust; our best-fit model for the hot dust actually overpredicts the measured 70 μm flux density and is slightly higher than the 1 σ upper limit at 160 μm (the 3 σ upper limit is plotted). The model does a reasonable job of reproducing the data for the issues we care about, namely, the dust location (temperature), the presence of small grains, and the crystallinity fraction.

- Liu, F. et al. 2008, *Proc. SPIE*, 7017
- Lovis, C., Mayor, M., Pepe, F., Alibert, Y., Benz, W., Bouchy, F., Correia, A. C. M., Laskar, J., Mordasini, C., Queloz, D., Santos, N. C., Udry, S., Bertaux, J.-L., & Sivan, J.-P. 2006, *Nature*, 441, 305
- Marinova, M. M., Aharonson, O., & Asphaug, E. 2008, *Nature*, 453, 1216
- Matranga, M., Drake, J. J., Kashyap, V. L., Marengo, M., & Kuchner, M. J. 2010, *ApJ*, 720, L164
- Melis, C., Zuckerman, B., Rhee, J. H., & Song, I. 2010, *ApJ*, 717, L57
- Meyer, M. R., Backman, D. E., Weinberger, A. J., & Wyatt, M. C. 2007, *Protostars and Planets V*, 573
- Meyer, M. R., Carpenter, J. M., Mamajek, E. E., Hillenbrand, L. A., Hollenbach, D., Moro-Martin, A., Kim, J. S., Silverstone, M. D., Najita, J., Hines, D. C., Pascucci, I., Stauffer, J. R., Bouwman, J., & Backman, D. E. 2008, *ApJ*, 673, L181
- Moór, A., Apai, D., Pascucci, I., Ábrahám, P., Grady, C., Henning, T., Juhász, A., Kiss, C., & Kóspál, Á. 2009, *ApJ*, 700, L25
- Press, W. H., Teukolsky, S. A., Vetterling, W. T., & Flannery, B. P. 1992, *Numerical recipes in C. The art of scientific computing*, 2nd edn. (Cambridge: University Press)
- Rhee, J. H., Song, I., & Zuckerman, B. 2008, *ApJ*, 675, 777
- Sogawa, H., Koike, C., Chihara, H., Suto, H., Tachibana, S., Tsuchiyama, A., & Kozasa, T. 2006, *A&A*, 451, 357
- Song, I., Zuckerman, B., Weinberger, A. J., & Becklin, E. E. 2005, *Nature*, 436, 363
- Strom, R. G., Malhotra, R., Ito, T., Yoshida, F., & Kring, D. A. 2005, *Science*, 309, 1847
- Su, K. Y. L., Rieke, G. H., Stansberry, J. A., Bryden, G., Stapelfeldt, K. R., Trilling, D. E., Muzerolle, J., Beichman, C. A., Moro-Martin, A., Hines, D. C., & Werner, M. W. 2006, *ApJ*, 653, 675
- Trilling, D. E., Bryden, G., Beichman, C. A., Rieke, G. H., Su, K. Y. L., Stansberry, J. A., Blaylock, M., Stapelfeldt, K. R., Beeman, J. W., & Haller, E. E. 2008, *ApJ*, 674, 1086
- van Leeuwen, F. 2007, *A&A*, 474, 653
- Weinberger, A. J. 2008, *ApJ*, 679, L41
- Wright, J. T., Marcy, G. W., Butler, R. P., & Vogt, S. S. 2004, *ApJS*, 152, 261
- Wyatt, M. C., Smith, R., Greaves, J. S., Beichman, C. A., Bryden, G., & Lisse, C. M. 2007, *ApJ*, 658, 569
- Zuckerman, B., Fekel, F. C., Williamson, M. H., Henry, G. W., & Munro, M. P. 2008, *ApJ*, 688, 1345